An engineering approach for the estimation of slewing bearing stiffness in Wind Turbine Generators

Iker Heras, Josu Aguirrebeitia, Mikel Abasolo and Ibai Coria

Department of Mechanical Engineering, University of the Basque Country, Bilbao, Spain

ABSTRACT

The stiffness of yaw and pitch slewing bearings has a critical influence on the structural behaviour of Wind Turbine Generators. Thus, it is commonly required by designers for their simulations to estimate deformations and select the most suitable bearing for their working conditions in preliminary design stages. In this work, a Design of Experiments was carried out via Finite Element Analysis to obtain the stiffness curves of all of the standard four-point contact slewing bearings from the catalogues of manufacturers under radial, axial and tilting loads. From these results, a set of simple formulas to calculate the ring deformations were adjusted. Combining them with contact deformation results obtained in previous work by the authors, a complete and efficient tool for slewing bearing stiffness estimation has been developed.

KEYWORDS

Bearing stiffness; Slewing bearing; Yaw bearing; Pitch bearing; Design of Experiments; Stiffness formulation.

Correspondence

Mikel Abasolo, Department of Mechanical Engineering, University of the Basque Country, Bilbao, Spain.
E-mail: mikel.abasolo@ehu.eus

1. INTRODUCTION

In Wind Turbine Generators (WTG), slewing bearings are used for orientation purposes (yaw bearing) and in the pitch control (blade bearings). These bearings are subjected to very specific working conditions, where small amplitude oscillatory rotations and high combined loads are involved. For these reasons, the selection criteria is complex and many factors need to be considered, like the static load capacity, the dynamic capacity and the fatigue behaviour or the friction torque.[1-3] Other specific phenomena must be also considered, like false brinelling and fretting corrosion.[4]

In this context, the global stiffness is a key parameter to account for the structural response of WTG under external static and dynamic loads. A good estimation allows the designers to calculate global deformations, and consequently predict possible interferences between adjacent components or unacceptably large displacements. For this reason, the global stiffness can also be subjected to certain specifications or criteria, since large values of the stiffness are required to minimize displacements.

Among the many structural components of WTGs, slewing bearings play a critical role in the stiffness, since they connect the tower to the nacelle and the hub to the blades. This means that an incorrect estimation of the stiffness of the slewing bearing will lead to underestimating or overestimating the structural response of the WTG. Even though Finite Element (FE) models are widely used to calculate stiffness, modelling simplifications are usually necessary to ensure convergence with a reasonable analysis cost. In this sense, in FE models of WTGs, rolling bearings are usually substituted by a stiffness matrix.

Being such an important design parameter, bearing stiffness is commonly required by customers to perform their simulations before selecting the most suitable bearing for their particular application; in some cases it is even available on manufacturer webpages.[5] Nevertheless, the calculation method is undisclosed, being part of the know-how of the manufacturer. Thus, an efficient way of calculating it would be a very powerful tool for WTG designers, because it would allow them to select the appropriate bearing by themselves, and then make direct comparisons between the solutions offered by different bearing manufacturers.

Several works have dealt with this issue. In some works ball load distribution was analytically calculated for four-point contact slewing bearings, from which load-deformation curves can be built;[1,6,7] similar methodologies were developed for two-point angular contact bearings.[8-13] However, all these works assume rigid rings, i.e. only ball-raceway contact deformations are considered, thus overestimating the bearing stiffness. Other semi-analytical and numerical models take into account the flexibility of the rings, but costly FE calculations are needed to calculate the stiffness matrix or to simulate ball load distribution, and the results are valid only for the particular bearing under study.[14-17] Neither is any formulation nor methodology for the stiffness estimation in any standard or guideline.[18-20]

This work presents a FE-based methodology to calculate the global stiffness of four-point contact slewing bearings, which leads to a set of formulas for the axial, radial and tilting stiffness. These simple formulas are proved to replicate the effect of main geometrical and contact parameters of all the standard bearings from the catalogues of manufacturers. In this sense, WTG designers can directly use them in early design stages as a fast and reliable alternative to more complex analytical approaches or computationally expensive numerical models.

2. MATERIALS AND METHODS

2.1. Fundamentals

The methodology is based on the fact that standard four-point contact slewing bearings fulfill certain geometrical relationships. As it is later demonstrated, the geometry is mainly defined by the mean diameter (D_{pw}), which gives the global size, and the ball diameter (D_w). The dimensions of the cross section of the bearing, the number of balls (N_b), the number of holes (N_h) and the bolt metric (M) that define the standard design can be quite accurately defined as a function of these main parameters D_{pw} and D_w.

Thus, the first step is to define the design space, that is, to identify the typical values of the main parameters for the standard bearings by studying the catalogues of the manufacturers,[21-25] in order to delimit the scope of the study. From this study, the standard design is defined. Then, a Design of Experiments (DOE) is performed via FE analyses, covering the design space by combining the values of the main parameters. As a result, load-deformation curves for each Design Point (DP) of the DOE and each load case (axial, radial and tilting moment) are obtained. The results are very accurate, because the FE model considers not only the effect of ball-raceway and ring deformations, but also other phenomena like flange-ring contact nonlinearities and bolt preload. Although FE calculations of the DOE are highly time consuming, the results have been used to achieve simple formulas of axial, radial and tilting stiffness for any bearing of the design space, which provide immediate results; these formulas will be a function of the main parameters. Additionally, the formulation has later been extended to further consider ball-raceway contact parameters (whose value does not depend on the main parameters) that also affect the bearing stiffness, namely the ball preload (δ_P), the conformity ratio (s), the initial contact angle (α), and the ball-filling ratio (R_{fill}).

It is worth pointing out that the studied load cases are pure axial, radial and tilting loads. Consequently, three formulas are obtained, one for each of them, leading to a diagonal stiffness matrix; load combinations are beyond the scope of this work. Even though slewing bearings must usually face combined loads, the obtained results still have a wide-range application field. Furthermore, this information is rarely offered by manufacturers or requested by WTG designers; in any case, out-of-diagonal terms in the matrix can be calculated by specific FE calculations.

2.2. Design space

The design space was defined from the study of the catalogues of Iraundi, SKF, Rothe Erde, Schaeffler and Lyc;[21-25] other manufacturers, like Rollix, do not include the dimensions of the ball in their catalogues.[26] The values of the main parameters D_{pw} and D_w for every four-point contact slewing bearing (over 200 bearings including regular and light series) were compiled and represented in the plot of Figure 1. Based on this point-cloud, the design space delimited by the upper and lower limiting curves was defined. Thus, it can be observed that this study covers every slewing bearing from the main manufacturers, embracing bearings with ball diameter between 15mm and 55mm, and mean diameter up to 3500mm. Based on the design space, the DOE in Figure 2 is proposed, consisting of 14 DPs. As mentioned, three FE calculations were made for each DP (one per load case), so the DOE comprises 42 calculations.

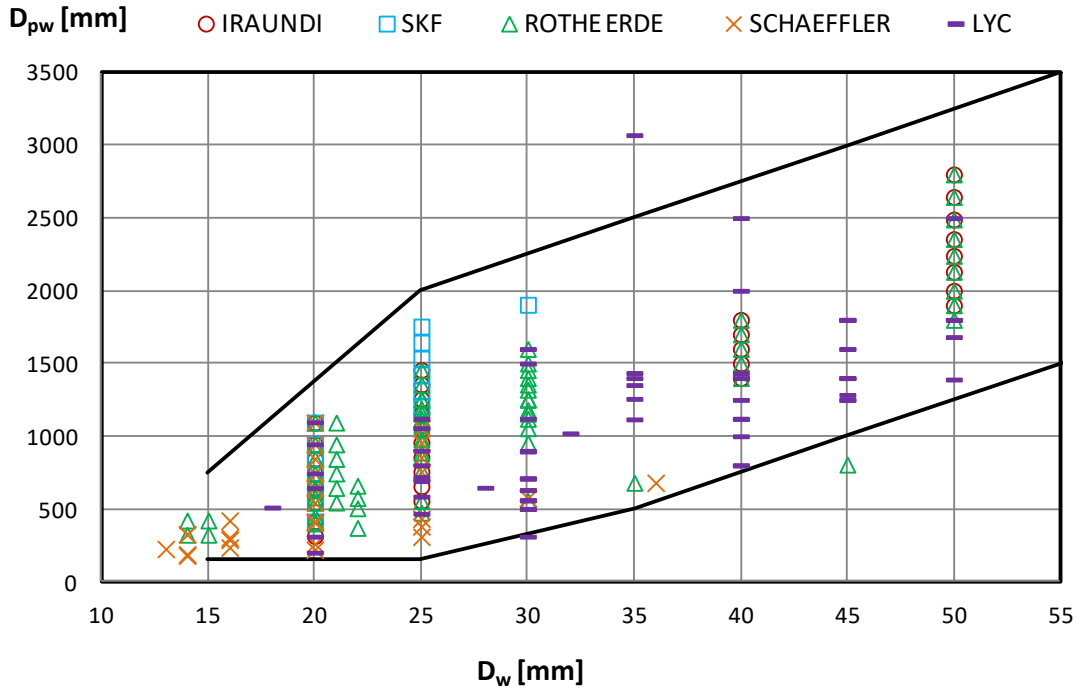

Figure 1. Values of the main parameters for slewing bearings of the main manufacturers, and definition the design space.

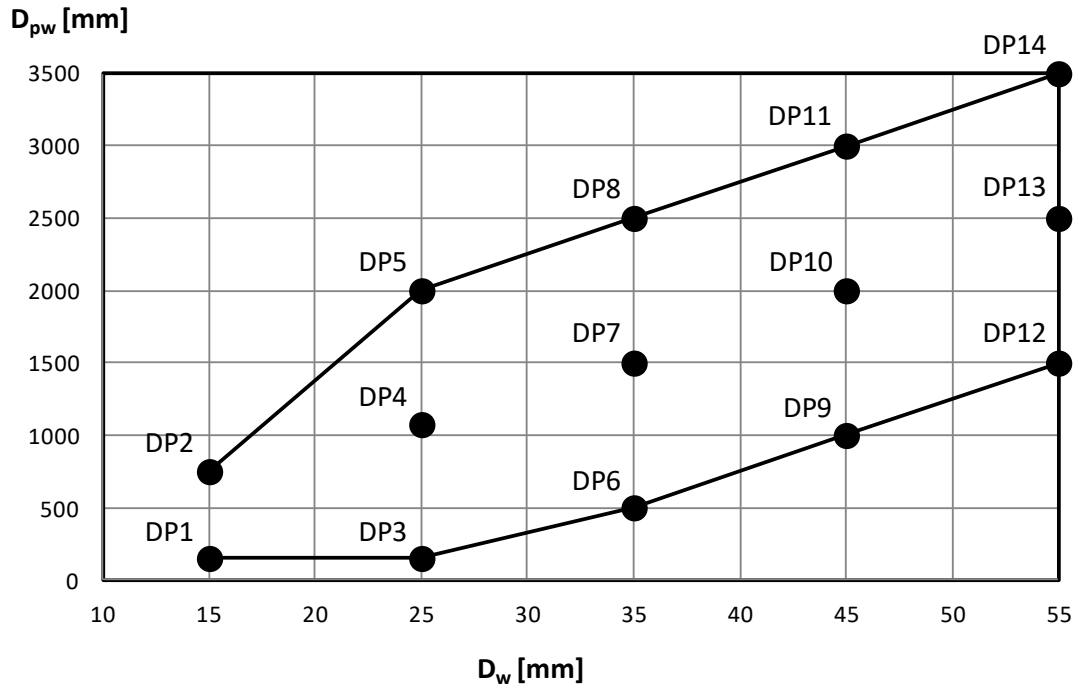

Figure 2. DOE for the design space.

2.3. Standard design

As a first approach, 90 standard series bearings from Iraundi and SKF catalogues were used. After defining the standard design, it was validated by contrasting it with bearings from the other manufacturers (see Figure 1). To reduce the number of parameters needed to define the standard design, the cross section was considered anti-symmetric, gears and threaded through bolt holes were not modelled, and finally the same number of bolt holes was modelled in both inner and outer rings. Such simplifications were demonstrated through preliminary FE calculations not to significantly affect the results. Figure 3 shows the sketch of the standard design section, which is defined by eight additional parameters: together with H_g, five of them define the dimensions of the cross section as a function of the ball diameter D_w via $R_H, R_L, R_{Lg}, R_{Lt}, R_{Dt}$ ratios; finally, s and α are contact parameters. Table 1 shows the non-contact parameter average values (very low scatter was found) calculated from the 90 bearings. Table 1 also shows the value for another coefficient, R_{Nh}, which relates the number of bolt holes (N_h) with the main parameters through the following expression:

$$N_h = R_{Nh}\frac{D_{pw}}{D_w} \tag{1}$$

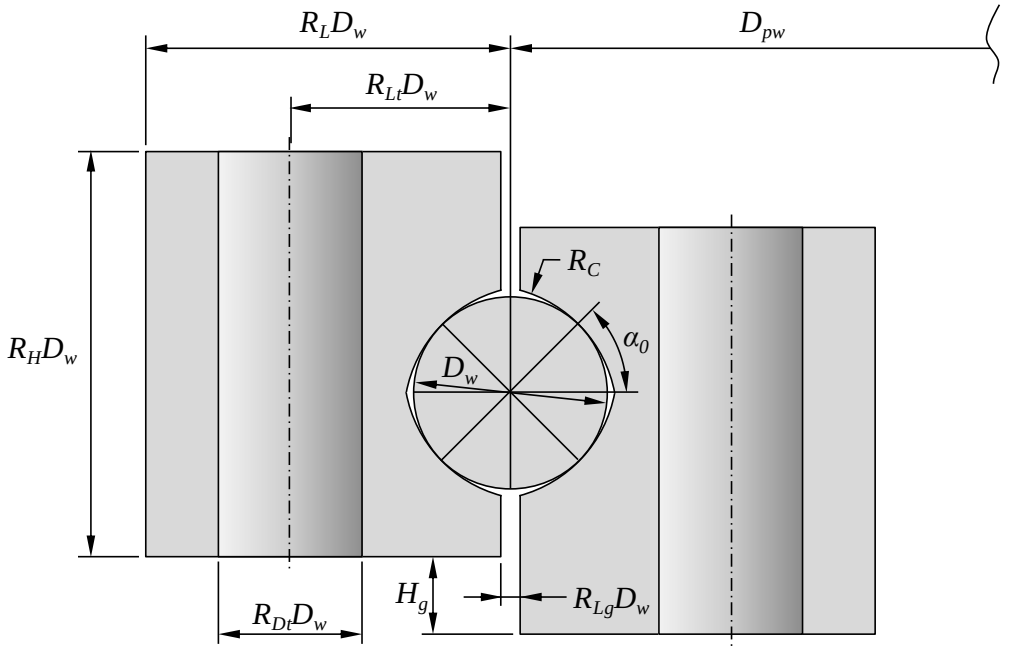

Figure 3. Sketch of the standard section.

R_H	H_g	R_L	R_{Lg}	R_{Lt}	R_{Dt}	R_{Nh}
2.15	10mm	1.9	0.1	1.15	0.75	1

Table 1. Dimensional values for the standard design parameters.

It is important to point out that, in bearings with diameters larger than the considered in this study (>3500mm), the absolute distance between the holes must be also checked for a proper bolted joint. Thus, in these cases the value of R_{Nh} as defined in (1) could adopt higher values. Nevertheless, these bearings are out of the scope of this manuscript.

Figure 4 compares the values from the catalogues (dots) with the values adopted for the standard design (lines). Subscripts a and i correspond to outer and inner rings respectively. Figure 5 shows the same comparison but only for the number of holes. These plots show that the proposed standard design satisfactorily fits the designs of Iraundi and SKF. As mentioned, the standard design was compared with other manufacturers' bearings, also achieving a good match.

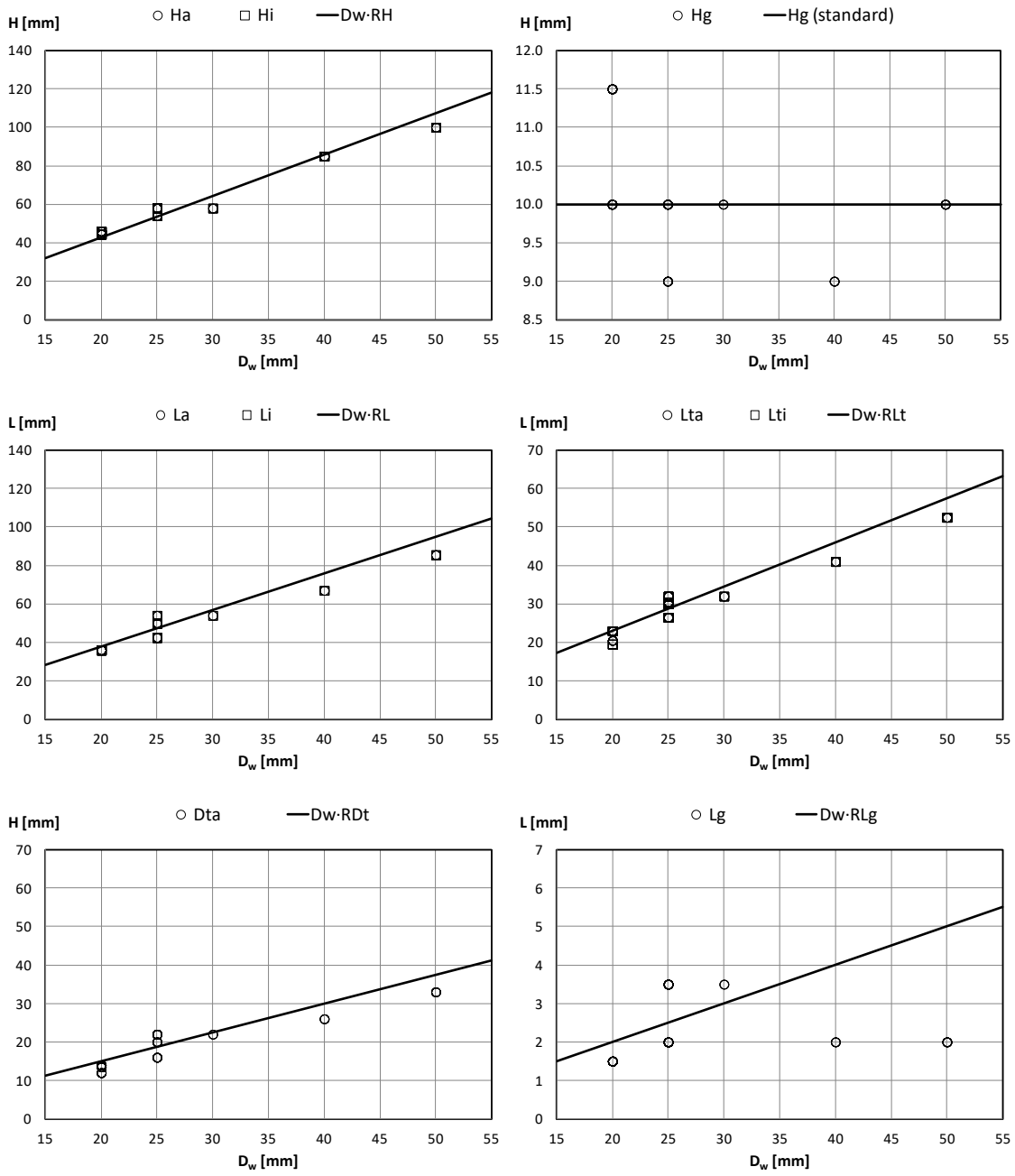

Figure 4. Standard section (lines) VS Catalogues (dots).

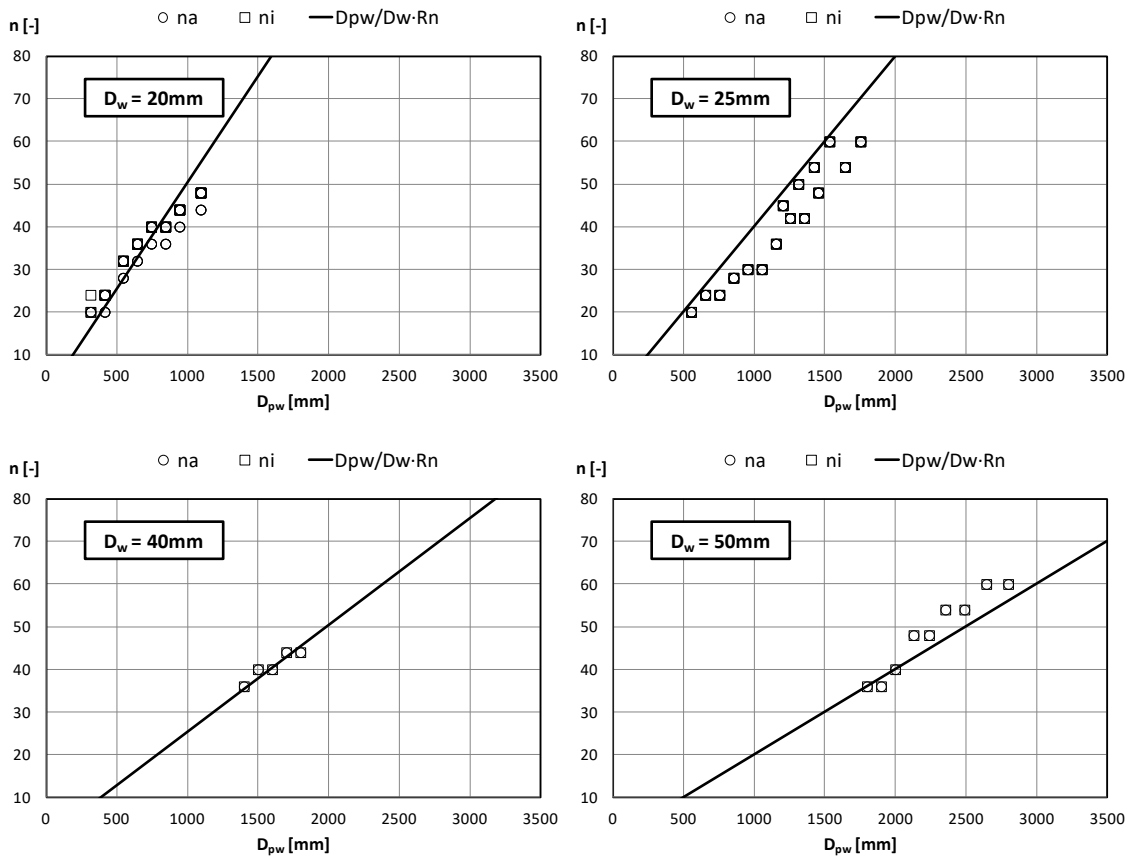

Figure 5. Number of holes: Standard design (lines) VS Catalogues (dots).

For contact parameters s and α, typical values of 0.943 and 45° were assumed, and no preload was considered. The ball number (N_b) is a function of the main parameters and the ball-filling ratio R_{fill}:

$$N_b = round\left[R_{fill} \cdot trunc\left(\pi \frac{D_{pw}}{D_w}\right)\right] \tag{2}$$

R_{fill} goes typically from 80% to 100%; for the first approach and before including contact parameters in the study, a value of 90% was assumed. Finally, a typical value of 75% of the yield stress is adopted for bolt preload. For the bolt metric, the following formula was considered, consistent with the bolts used according to the catalogues:

$$M = 2 \cdot trunc\left(\frac{D_t - 1.5}{2}\right) \tag{3}$$

2.4. Finite Element model

A fully parametric FE model has been generated in ANSYS® Workbench in order to perform the analyses and process the results in an automated way, for any geometry and load condition. APDL scripts were required to address some limitations of the Workbench environment.

Due to the symmetry of the geometry and the loads, only half the bearing was modelled. Although simplified ball models based on springs are widely used to save computational cost,[12,13] they have limitations for radial load cases. When radial loads are applied, those springs leave the radial plane introducing an artificial radial stiffness. For this reason, solid balls are used. The bearing is bolted to flanges to prevent rings from deforming freely. The flanges are rigid, thus simulating rigid adjacent structures, for two reasons: on the one hand, the structures can be significantly different depending on the application; on the other hand, the aim of the study is to calculate the stiffness of the bearing, without the effect of the surrounding components. In this sense, assuming rigid rings is not a limitation of this work, because the flexibility of the surrounding structures can be later considered in further calculations, where the bearing would be simplified by means of the formulas derived from the current study.

In order to avoid excessive cost while ensuring analysis convergence, special attention was paid to the meshing process. The geometry was divided into sweepeable bodies and the element size was defined as a function of the ball diameter, so as to obtain a refined mesh in the contact area without introducing elements with low aspect ratio. Figure 6 shows a detail of the mesh for a particular bearing, with the different bodies in different colours, including the flanges. Solid components (rings, balls and flanges) are meshed with solid elements, were hexahedrons are dominant. Bolts are modelled by beam elements with pretension section joined to the rings and the flanges by rigid links, all of them introduced via parametric APDL script (see Figure 7a). The mesh was proved to offer reliable results with affordable computational costs. Regarding contacts, frictional contact is defined for the ball-raceway contact, with a coefficient of friction of 0.1;[27,28] ring-flange contact is frictional too, with a coefficient of friction of 0.3, allowing the sliding or the opening of the joint. Finally, a bonded contact is defined between the different bodies of the rings with a pure penalty formulation (see Figure 6).

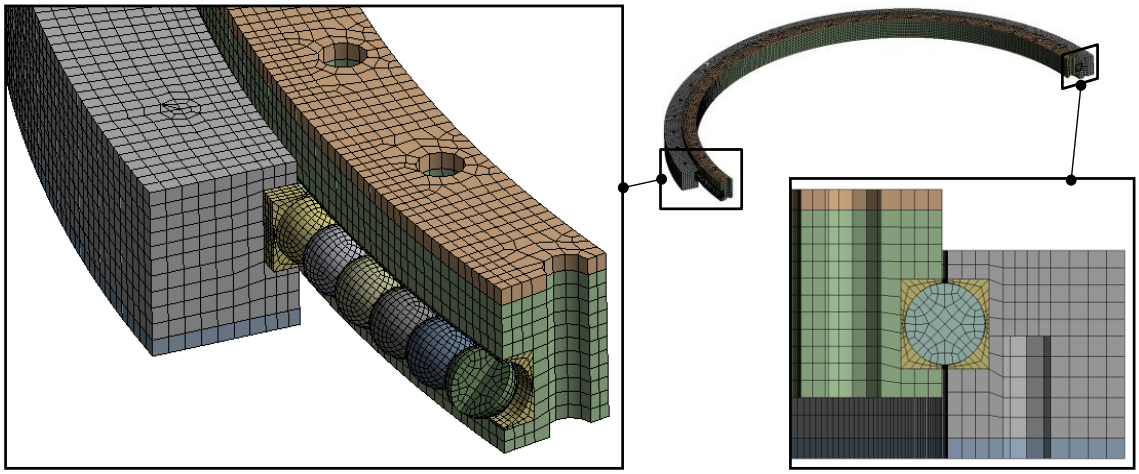

Figure 6. FE mesh for the Iraundi POS214-8 bearing.[21]

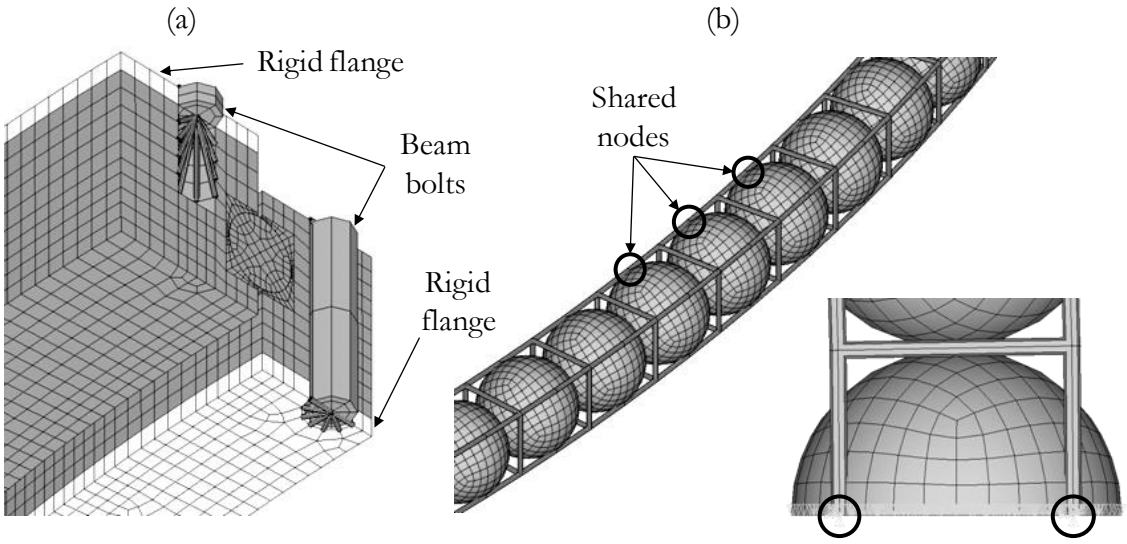

Figure 7. FE model details introduced via APDL scripts: a) bolt b) cage.

To simulate the symmetry of the model, frictionless boundary conditions are imposed on the faces on the symmetry plane. The outer flange of the bearing is fixed, while the displacements are applied to the inner flange through a remote node placed in the centre of the bearing and at the height of the interface between the flange and the ring. The loads that correspond to the imposed displacements are obtained by evaluating the reaction forces in the aforementioned remote point.

In the simulation, large displacements are involved, mainly due to the variation of the ball-raceway contact angle. This fact, together with the ball-raceway and ring-flange frictional contacts, makes the model highly nonlinear. The model showed important convergence problems due to the ball-raceway contacts, mostly in the first load steps when some balls lose the contact and become unconstrained. This problem is especially notorious when a pure radial load is applied, where half the balls lose the contact. This is a common problem in ball bearing simulations, but no method was found in the literature to deal with it. Therefore, a new modelling alternative was developed, consisting of the cage formed by thin beams shown in Figure 7b. As indicated in the figure, the beams share nodes with the balls (but not with the rings), thus linking the balls to each other. This structure ensures the convergence with no loss of accuracy, because its stiffness is negligible. The number of the degrees of freedom of the model varies depending on the dimensions of the bearing, ranging from around $2.6 \cdot 10^5$ for low D_{pw}/D_w ratios to $3.6 \cdot 10^6$ for high D_{pw}/D_w ratios. The simulation cost varied from 1 hour for low D_{pw}/D_w ratios to 1 day for high D_{pw}/D_w ratios in a high performance work station (Intel® Xeon® E5-2697 v3 @ 2.6GHz processor with 14 physical cores – 28 logical – and a RAM of 128GB).

3. RESULTS AND DISCUSSION

3.1. DOE results

As shown in Figure 2, the DOE consisted of 14 DPs. Figure 8 shows the axial, radial and tilting stiffness curves for one of them, DP7; nevertheless, all comments and derived conclusions are applicable to any other DP. In red dots the axial and radial forces, as well

as the tilting moment, are shown for increasing values of the applied displacements; in blue lines, the stiffness for each load step can be seen. Note that the blue stepped curve (the stiffness) represents the slope between adjacent red points (force-displacement points) for each load step. These lines evinced the discontinuity in the tendency of the resistant behaviour of the bearing. In each load case, a clear jump in the stiffness was observed, pointing to the load value from which this behaviour changes. Contrasting these curves with deformation and contact results (pressure and contact status) in the flange-ring joints, it was identified that this change in the tendency is due to contact nonlinearities. Figure 9 shows how flanges start either sliding (for axial or radial load) or opening (under tilting moment) after a threshold displacement. The effect of this nonlinearity is out of the scope of the study in order to achieve generally applicable conclusions and results, because this threshold value depends on the stiffness of the adjacent structures and the bolt preload level. Moreover, in the FE model, the flanges are infinitely rigid, favouring a premature opening. For these reasons, only the values below the threshold displacement were considered for the stiffness calculation.

Figure 10 compares the results for rigid and deformable rings to demonstrate the effect of the flexibility of the rings on the bearing stiffness. The results for rigid rings were obtained through the analytical model by the authors.[1] From the figure, it is concluded that rigid ring assumption largely overestimates the stiffness of the bearing, especially for large bearings. As an illustrative example, for 35mm ball, the displacements due to ring flexibility accounted for 36% of the total displacement in the smallest bearing (DP6), 47% in the medium-sized one (DP7) and 52% in the largest (DP8).

3.2. Functional approximation for ring stiffness

According to Hertz theory,[8] the relationship between the normal load (Q) and the local deformation (δ) in the ball-raceway contact is:

$$Q = K\delta^{1.5} \tag{4}$$

Based on this expression, the following formulas can be proposed for a first tentative approximation to the FE results, establishing a relationship between the applied loads F_a, F_r and M_t, and the corresponding displacements δ_a, δ_r and θ_t:

$$\begin{aligned} F_a &= K_a\delta_a^{n_a} \\ F_r &= K_r\delta_r^{n_r} \\ M_t &= K_t\theta_t^{n_t} \end{aligned} \tag{5}$$

Where subscript a is for axial, r for radial and t for tilting. In this case, the values of the exponentials are not 1.5 as in the normal contact problem in equation (4). It is important to emphasize that the objective of this manuscript is to obtain an engineering approach, i.e. a simple formulation that represents the structural behaviour of the bearing. The study of the real physics of the problem is beyond the interest of this work.

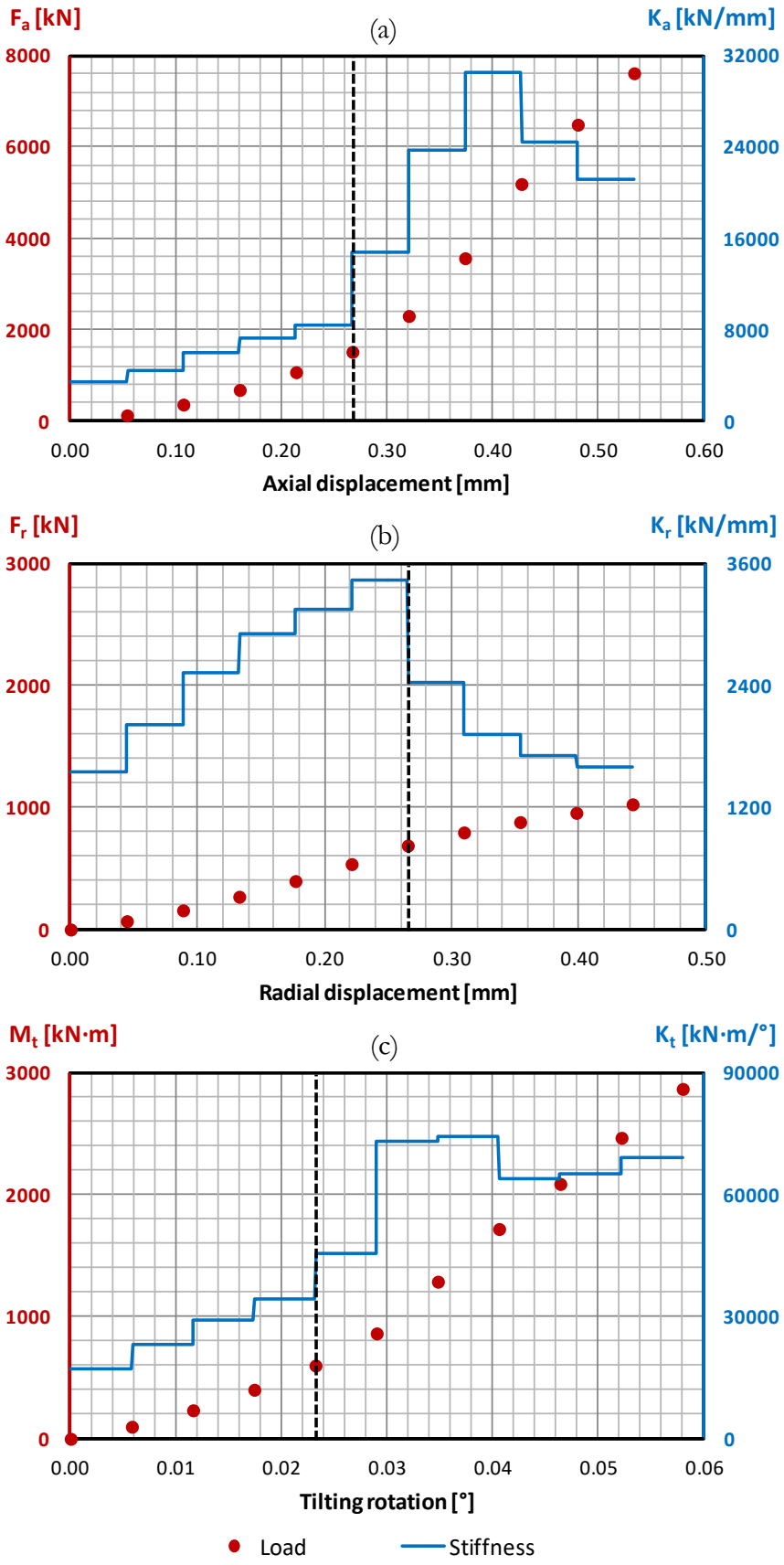

Figure 8. FE results for forces and moments (red dots) and stiffness (dashed blue curve): (a) for axial load; (b) radial load; (b) tilting moment.

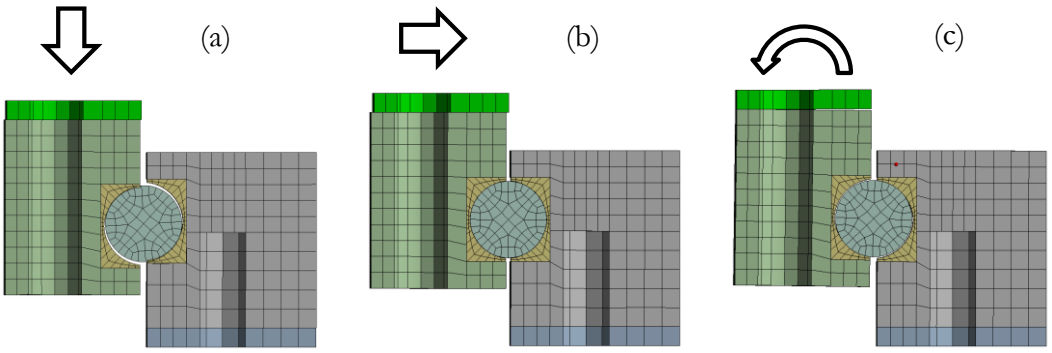

Figure 9. Nonlinear behaviour of the bolted joint (enlarged displacements): (a) with axial load; (b) radial load; (c) tilting moment.

The proposed approach to the bearing global stiffness estimation lies in separately calculating the displacements due to contact deformations and those due to the flexibility of the rings. Thus, the problem was decoupled so that each contribution was calculated separately. Hence, the total displacements were formulated as follows:

$$\delta = \delta_{contact} + \delta_{rings} \tag{6}$$

The aim of decoupling the problem was to consider separately the effect of the different parameters on the stiffness. By doing this, contact parameters such as ball preload or conformity ratio only affect $\delta_{contact}$ as described in the analytical model by the authors.[1] On the other hand, δ_{rings} is affected by the rest of the geometrical parameters, being D_w and D_{pw} the main ones.

Thus, a functional approximation based on equation (5) was proposed for the formulation of δ_{rings}, where K is a function of D_w and D_{pw}:

$$F = K\delta_{rings}^{n} = K\left(D_w, D_{pw}\right)\delta_{rings}^{n} \tag{7}$$

Where F can be F_a, F_r or M_t and δ_{rings} can be δ_a, δ_r or θ_t, depending on the load case under study. Finally, K was adjusted to fit all the results from the DOE. As FE results provide total deformation results (δ), and according to equation (6), δ_{rings} were obtained from deducting $\delta_{contact}$ values of the analytical model.[1] Then, the function (7) was approximated for each DP, obtaining the values of K and n for each load case, and it was found out that the coefficient n was very similar for every DP (under the same load case). In a second step, the value of n was fixed and K was recalculated to fit the stiffness curve. Figure 11 shows the results of this procedure. It can be observed that the effect of D_{pw} in the coefficient K is exponential; no such clear tendency was deducted for D_w.

Having tested different options, the most suitable functional form for K with the minimum number of coefficients was found to be:

$$K\left(D_w, D_{pw}\right) = C_w D_w^{n_w} + C_{pw} D_{pw}^{n_{pw}} \tag{8}$$

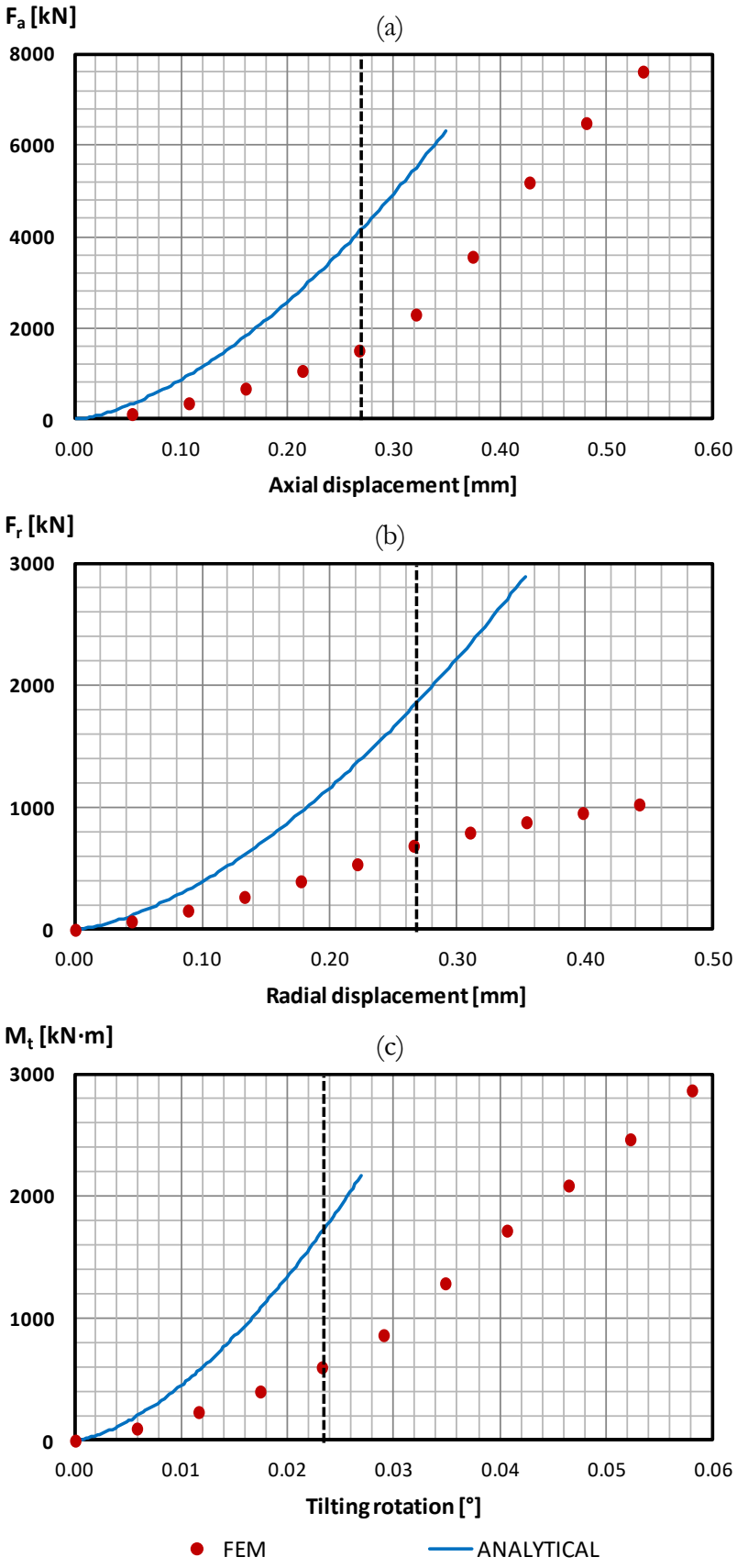

Figure 10. FE results (red dots) and analytical model results (blue curve) for DP7: (a) for axial load; (b) radial load; (b) tilting moment.

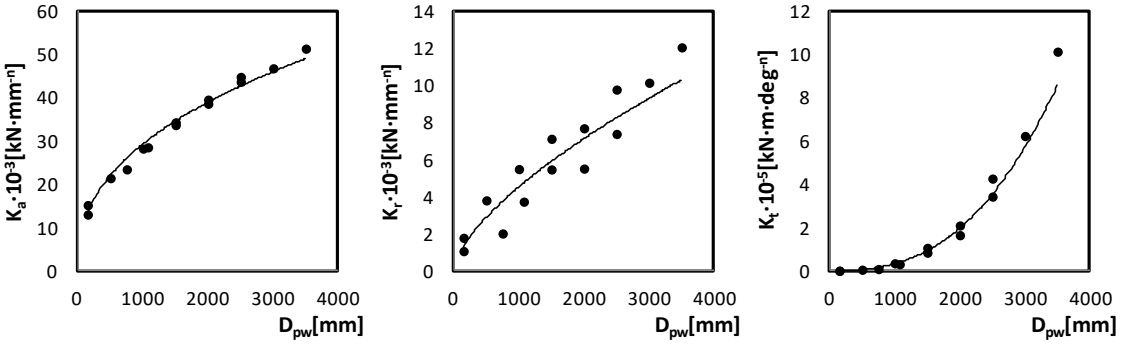

Figure 11. Tendencies of $\boldsymbol{K}$ coefficients with bearing mean diameter.

The expression for δ_{rings} was then obtained from (7) and (8):

$$\delta_{rings} = \left[\frac{F}{K\left(D_w, D_{pw}\right)}\right]^{\frac{1}{n}} = \left[\frac{F}{C_w D_w^{n_w} + C_{pw} D_{pw}^{n_{pw}}}\right]^{\frac{1}{n}} \tag{9}$$

Finally, the values of the 5 coefficients in (9) (n, C_w, n_w, C_{pw} and n_{pw}) that fit the curves for every DP were found. To this end, the Mean Weighted Relative Square Error ($MWRSE$) was defined as:

$$MWRSE = \frac{1}{N}\sum_{i=1}^{N}\left[\frac{1}{M_i}\sum_{j=1}^{M_i}\left[\frac{\left[\delta_{FE}^{ij} - \left(\delta_{contact}^{ij} + \delta_{rings}^{ij}\right)\right]^2}{\left(\delta_{FE}^{ij}\right)^2}\right]\right] \tag{10}$$

Where N is the number of DPs (14 in this case) and M_i is the number of points from the FE results for DP i before the nonlinearity of the joint occurs. By minimizing this error through the Newton-Raphson method, the values of the coefficients were obtained. Although a quadratic error was used for the minimization in order to favour the convergence, the Weighted Absolute Relative Error ($WARE_i$) gave a more intuitive idea of the error for each DP:

$$WARE_i = \frac{1}{M_i}\sum_{j=1}^{M_i}\left|\frac{\delta_{FE}^{ij} - \left(\delta_{contact}^{ij} + \delta_{rings}^{ij}\right)}{\delta_{FE}^{ij}}\right| \tag{11}$$

Table 2 shows the final values of the coefficients for each load case together with the mean value of the $WARE_i$ ($MWARE$). The units for C_w and C_{pw} are $\left[kN \cdot mm^{-(n-n_w)}\right]$ for axial and radial loads, and $\left[kN\, m \cdot mm^{-n_w}\right]$ for tilting moment. As can be seen, the error is less than 5% in any case.

Substituting the values from Table 2 in (8), the final formulas for the contribution of the rings to the total displacements were obtained, whose units are shown in Table 3:

$$\delta_a|_{rings} = \left[\frac{F_a}{3300 D_{pw}^{0.35}}\right]^{\frac{1}{1.6}}$$

$$\delta_r|_{rings} = \frac{F_r}{45 D_w^{1.2} + 0.15 D_{pw}^{1.3}} \tag{12}$$

$$\theta_t|_{rings} = \left[\frac{M_t}{53 D_w^{4.5} + D_{pw}^{3.1}} 10^5\right]^{\frac{1}{1.1}}$$

It is important to remark that these equations are valid and offer reliable results for any of the studied DPs, so they can be used to estimate the global stiffness of any bearing within the defined design space.[29] Figure 12 summarizes the results for DP7: in red dots, the total displacement values from the DOE; in blue lines, the contact deformation results from the analytical model;[1] in green lines, ring deformation values according to the proposed equations (12); finally, red lines are the summation of blue and green lines, i.e. total displacement, demonstrating that the proposed formulation for ring stiffness calculation accurately fits the DOE results. For this DP, the $WARE_i$ was 0.36%, 2.29% and 4.44% for axial, radial and tilting cases respectively, so it is a representative DP considering the mean values of the errors in Table 2.

	n	C_w	n_w	C_{pw}	n_{pw}	$MWARE$
Axial load	1.6	0	1	3300	0.35	1.5%
Radial load	1.0	45	1.2	0.15	1.3	3.5%
Tilting moment	1.1	$5.3 \cdot 10^{-4}$	4.5	10^{-5}	3.1	4.9%

Table 2. Values for the coefficients of the functional approximation for δ_{rings} and the relative error (MWARE).

F_a and F_a	M_t	δ_a and δ_a	θ_t	D_w and D_w
kN	$kN \cdot m$	mm	deg	mm

Table 3. Units for equation (12).

3.3. Extension of the formulation for contact parameters

As explained in the previous section, the aim of separating contact deformations and ring deformations in (6) was to be able to reproduce the effects of contact parameters in the global stiffness of the bearing without affecting the ring stiffness formulation (12). In this sense, it was assumed that contact parameters had an influence only on ball-raceway contact deformations. Additional FE calculations were performed to prove this hypothesis, and the results were compared with the ones from the proposed formulation.

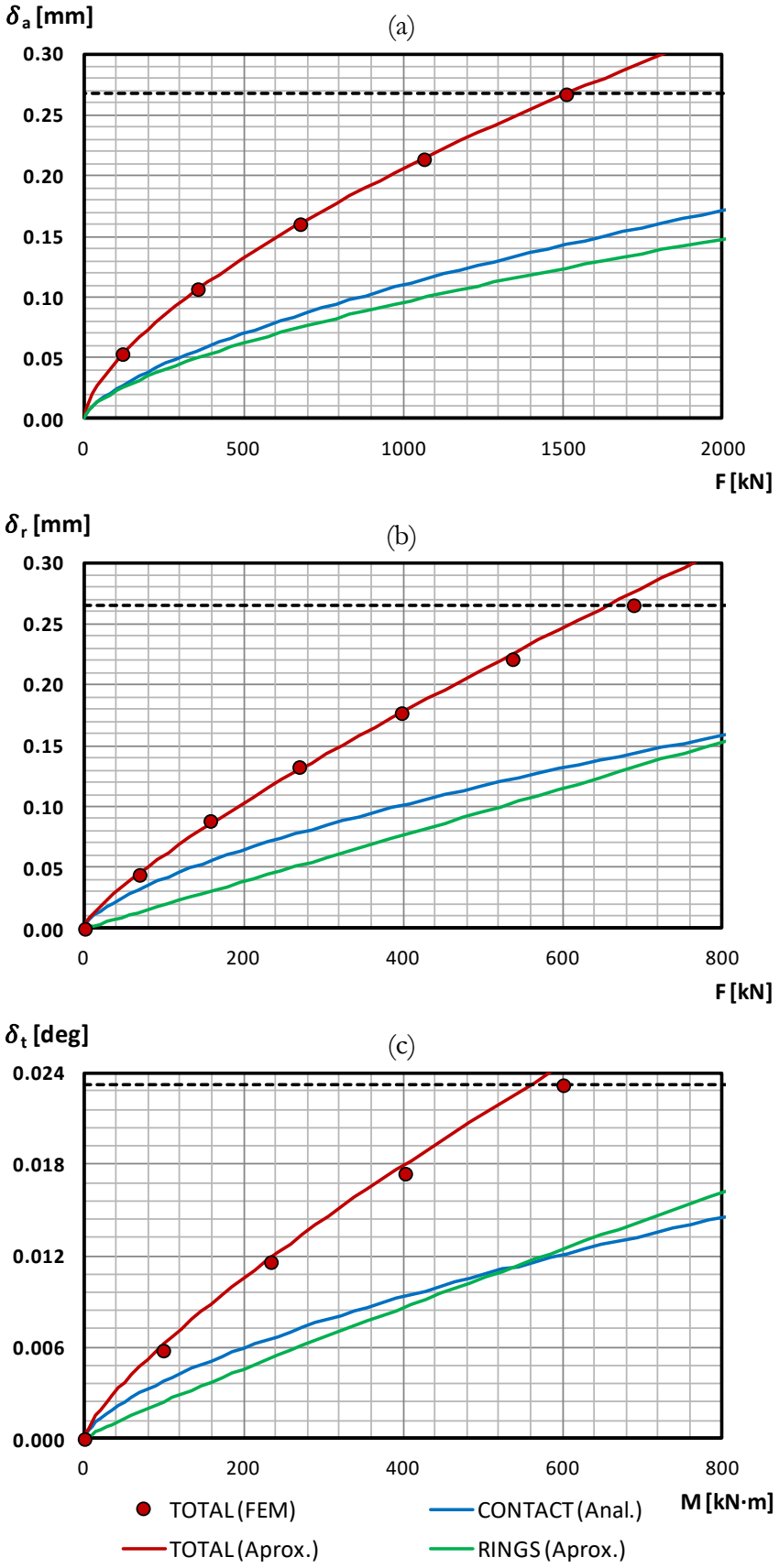

Figure 12. Analytical model results (blue curve), functional approximation for rings deformation (green curve), the summation of both curves (red curve) and FE results (red dots) for DP7: (a) for axial load; (b) radial load; (b) tilting moment.

The parameters related to the contact deformations are ball preload (δ_P), ball number (N_b), conformity ratio (s) and initial contact angle (α). Although the ball number is not a contact parameter, it affects the contact deformations because the more balls there are, the more contacts there will be. To verify that these parameters affect $\delta_{contact}$ and not δ_{rings}, different FE calculations were carried out varying their values for reference bearing DP7, studying the effect of each parameter separately.

For the preload, four different values were considered up to 10% of the static load capacity, which happens at 30μm for DP7, with the results shown in Figure 13; it can be seen that the curves from the proposed methodology are near the FE results, although they have limitations for high loads. The ball number is quantified by the filling ratio (R_{fill}) from formula (2), with the values for this ratio varying from 80% to 100%. In this case, three values were analysed; the results are shown in Figure 14 and the numerical errors are summarized in Table 3. As with the preload, the proposed methodology lacks accuracy as the load increases, but the values of the errors are still satisfactory. For the conformity ratio, values of 0.92, 0.943 and 0.96 were analysed; even though the formulation catches the tendency adequately (see Figure 15), the errors are larger than for the other parameters (Table 3). Finally, the effect of the initial contact angle was studied. For this purpose, values of 35°, 45° and 55° were considered. If the proposed formulation is applied without introducing any correction (dashed curves in Figure 16), the curves are far from the FE results, even though the tendency is correct. Nevertheless, a correction can be easily made using the γ factor, leading to the curves in solid lines, which show a good correlation with FE results. This correction factor comes from the unprojection of contact forces in the vertical axis for axial and tilting cases, and in the horizontal axis for the radial case:

$$F = \gamma \cdot K\left(D_w, D_{pw}\right)\delta_{rings}^{n} \quad \text{where} \begin{cases} \gamma_{a/t} = \frac{sin\alpha}{sin45^\circ} = \sqrt{2}\, sin\alpha \\ \gamma_r = \frac{cos\alpha}{cos45^\circ} = \sqrt{2}\, cos\alpha \end{cases} \tag{13}$$

Table 3 indicates the errors for the different contact parameters according to Figures 13 to 16. The values are near those for the nominal case previously pointed out in Table 2.

	δ_P	N	s	α
Axial load	1.7%	3.3%	6.8%	7.4%
Radial load	3.2%	3.3%	5.6%	3.7%
Tilting moment	5.5%	5.2%	7.5%	5.6%

Table 3. Relative error (MWARE) for the different contact parameters.

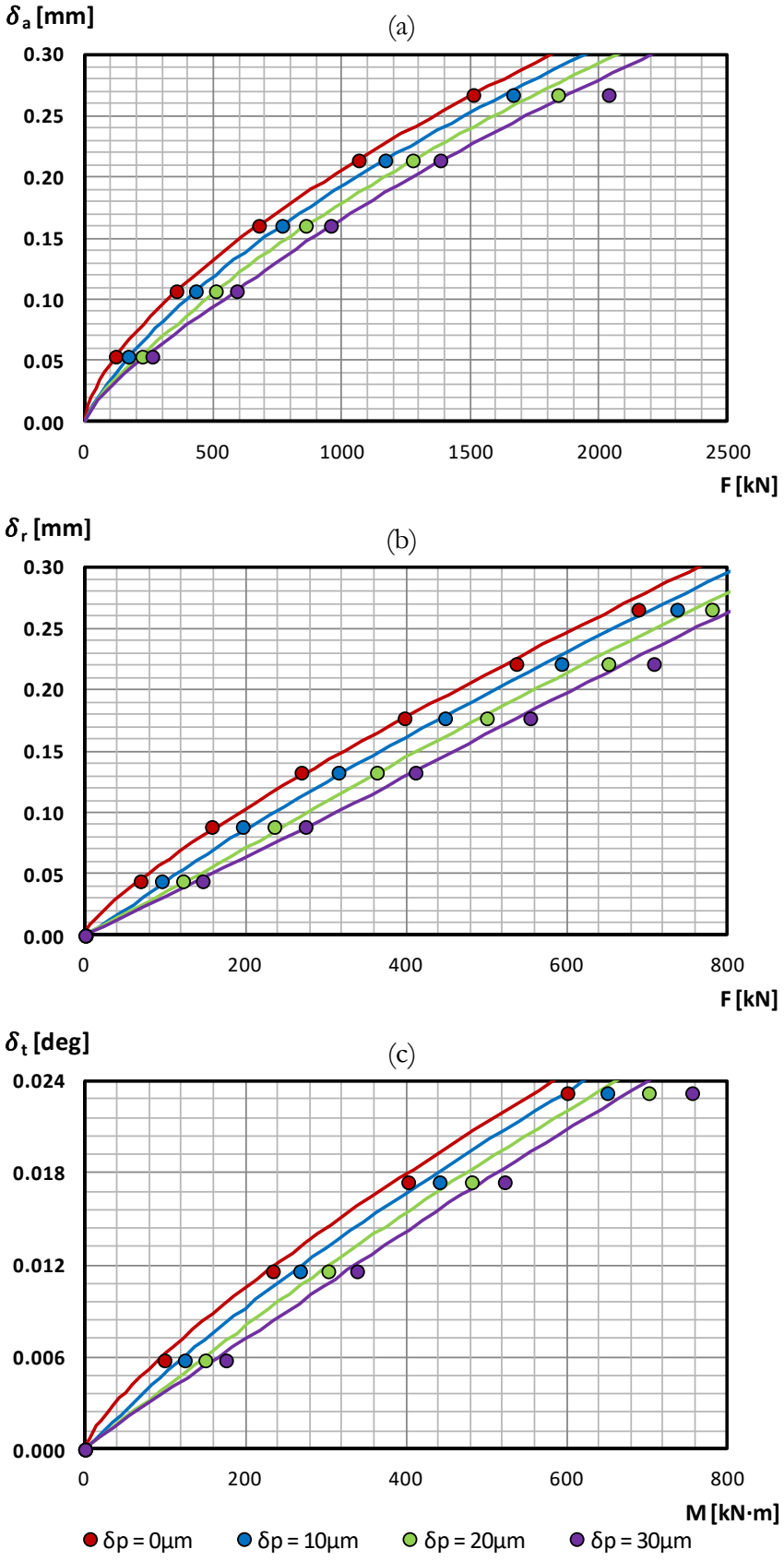

Figure 13. Effect of the preload according to the proposed formulation (curves) and FE results (dots) for DP7: (a) under axial load; (b) radial load; (b) tilting moment.

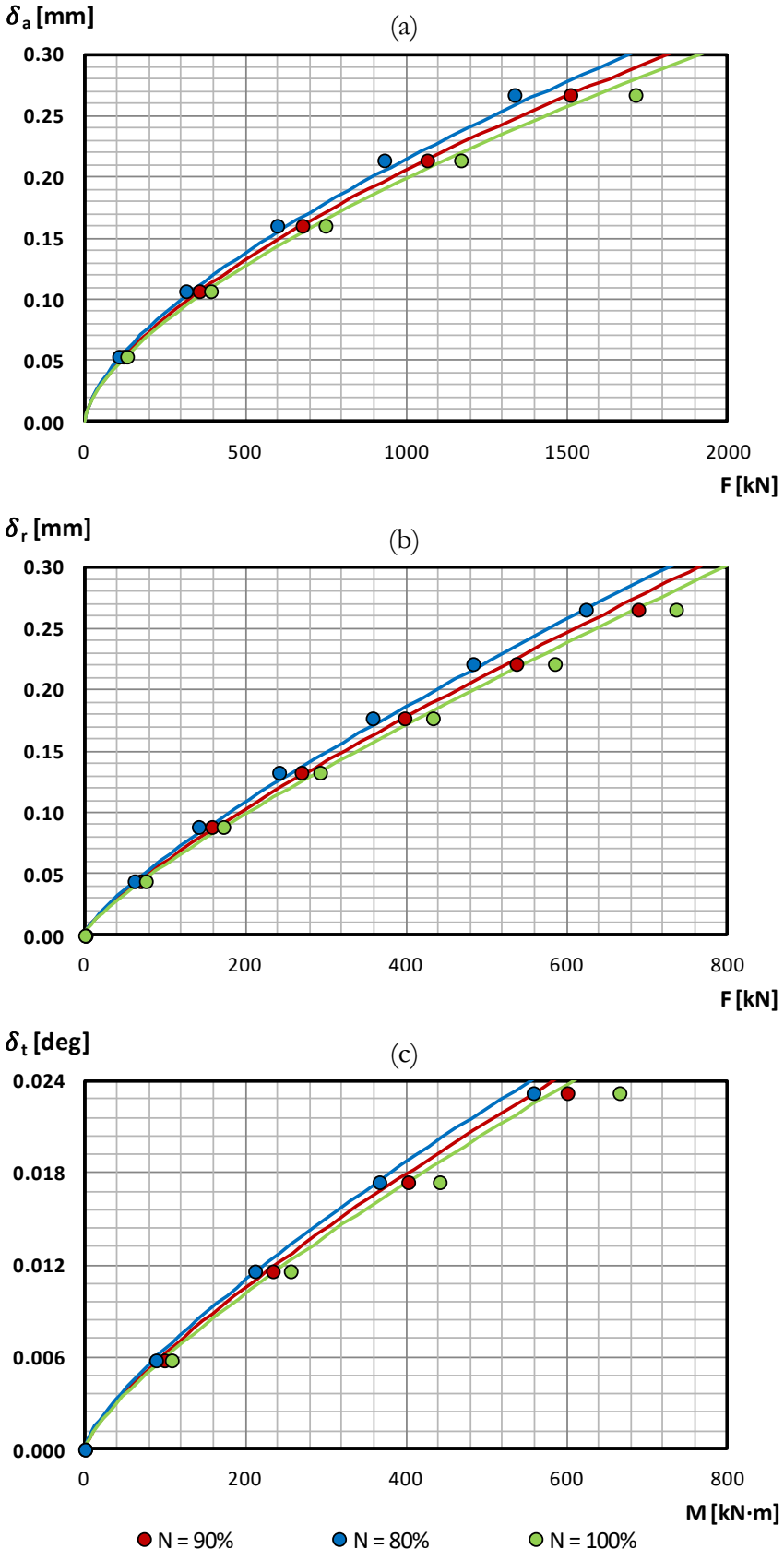

Figure 14. Effect of the ball number according to the proposed formulation (curves) and FE results (dots) for DP7: (a) under axial load; (b) radial load; (b) tilting moment.

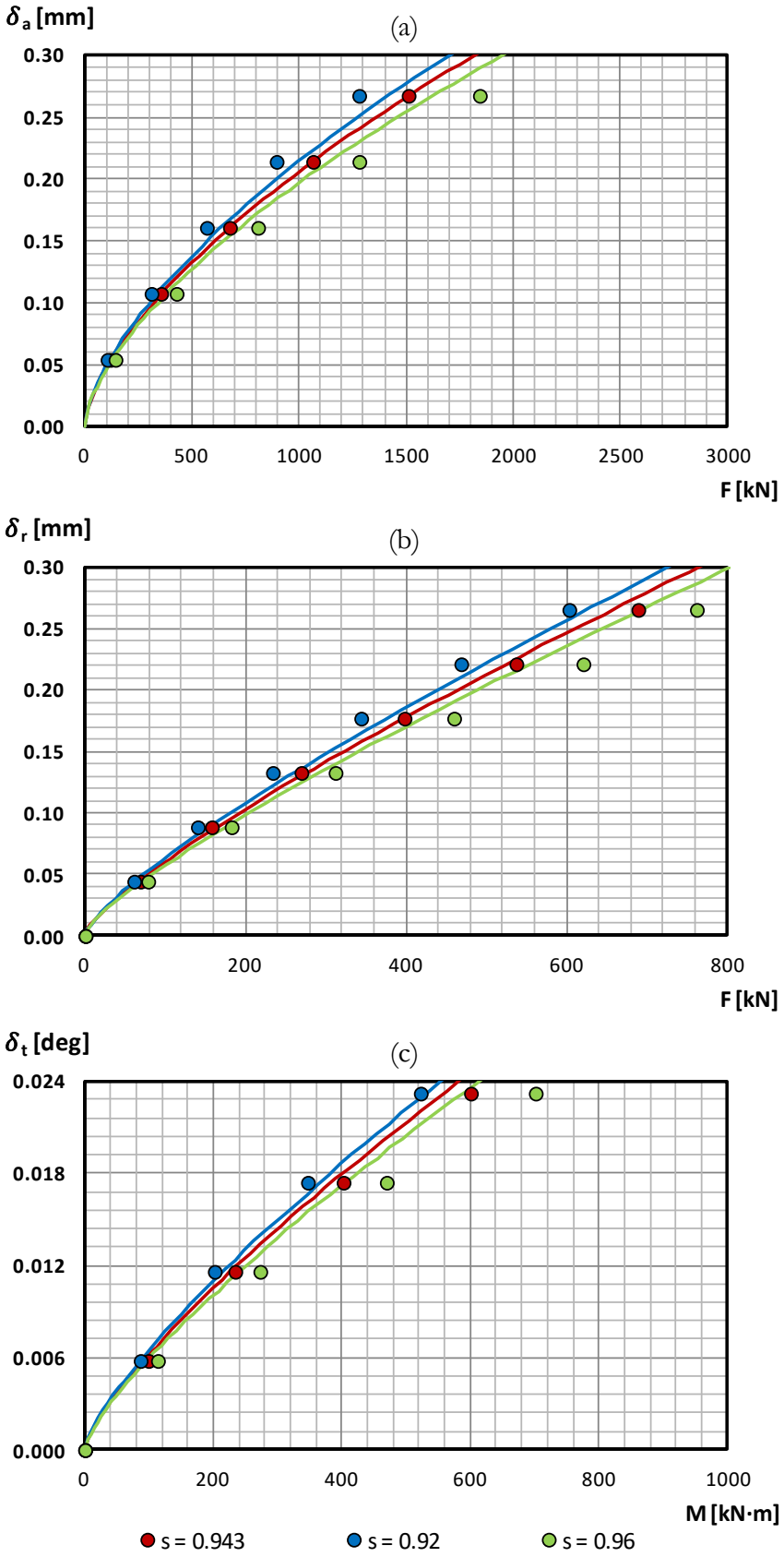

Figure 15. Effect of the conformity ratio according to the proposed formulation (curves) and FE results (dots) for DP7: (a) under axial load; (b) radial load; (b) tilting moment.

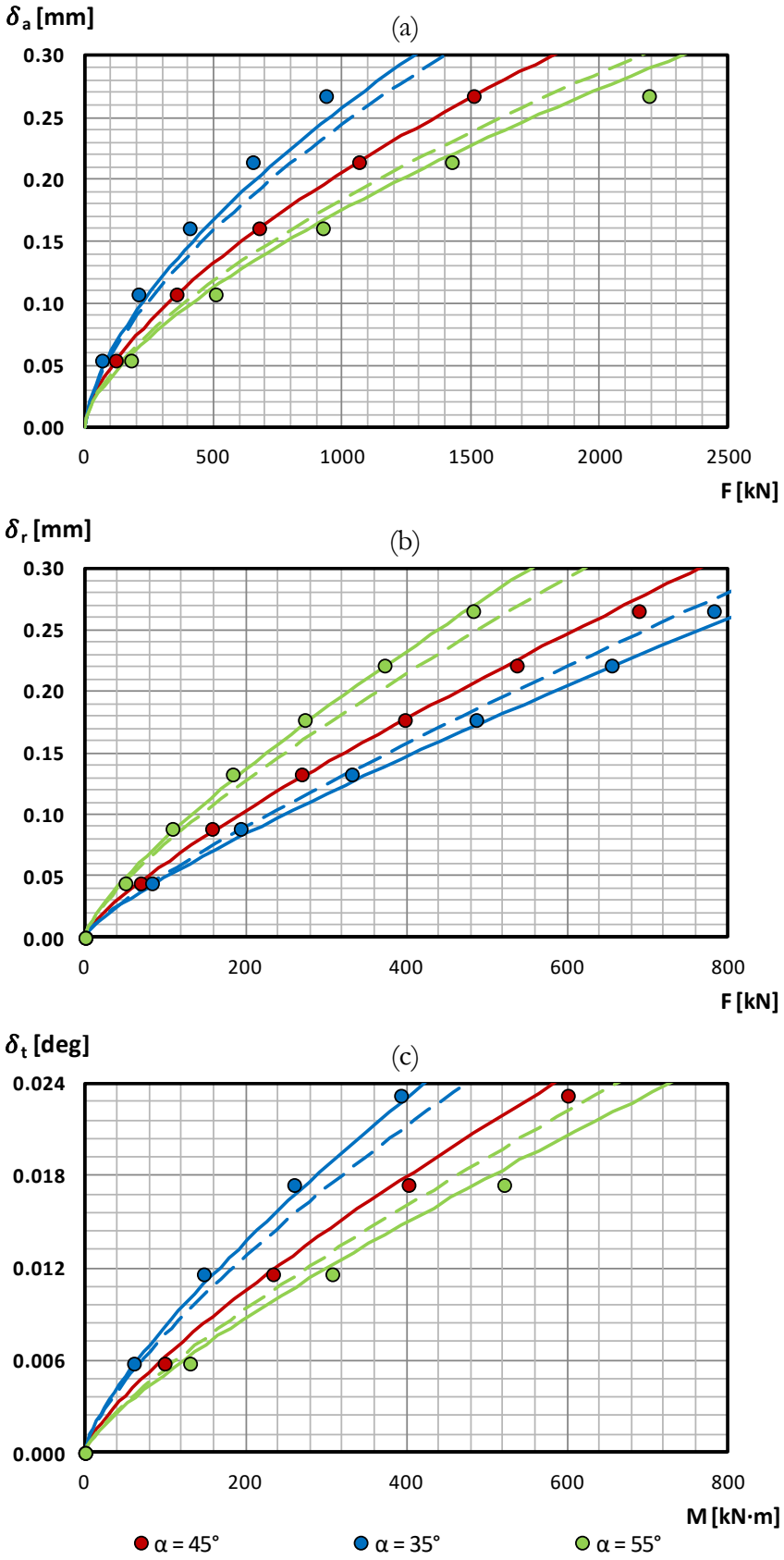

Figure 16. Effect of initial contact angle according to the proposed formulation without the correction (dashed curves), corrected (continuous curves) and FE results (dots) for DP7: (a) under axial load; (b) radial load; (b) tilting moment.

4. CONCLUSIONS

This work presents a procedure to calculate stiffness curves for four-point contact slewing bearings of Wind Turbine Generators, under external axial and radial forces, and tilting moments. For such purpose, the methodology separates ball-raceway contact deformations and ring deformations. While contact deformations can be calculated by analytical models found in the specialized literature, no simple and generalist procedure exists to calculate the effect of the flexibility of the rings. For such purpose, a Design of Experiments is performed with a parametric Finite Element model, and a set of stiffness formulas are derived from its results, which replicate the effect of the geometrical parameters of the standard four-point contact slewing bearings of manufacturers. Later, the formulas are combined with an analytical model by the authors to further consider contact parameters, showing good correlation with Finite Element results.

As a result, the proposed formulation is a fast and accurate tool to calculate the stiffness of standard four-point contact slewing bearings, taking into account both contact and ring deformations. It is an extremely useful approach not only for bearing manufacturers, but also for Wind Turbine Generator designers to feed their static and dynamic simulation models in preliminary design stages. The methodology was successfully applied to single-row four-point contact bearings, but it can be extended to other types of WTG slewing bearings such as double row four-point contact ball bearings and crossed roller bearings. In future works, the suitability of this method for the simulation of real pitch or yaw systems will be studied, considering realistic combined loads and possible nonlinear boundary effects.

ACKNOWLEDGEMENTS

This paper is a result of the close collaboration that the authors maintain with the company Iraundi S.A. This work was supported by the Ministry of Economy and Competitiveness of Spain [project number DPI2013-41091-R], the Basque Government [Grant Number IT947-16] and the University of the Basque Country (UPV/EHU) [project number UFI 11/29].

REFERENCES

1. J. Aguirrebeitia, J. Plaza, M. Abasolo, J. Vallejo, Effect of the preload in the general static load-carrying capacity of four-contact-point slewing bearings for wind turbine generators: theoretical model and finite element calculations, Wind Energy. 17 (2014) 1605–1621. doi:10.1002/we.1656.

2. F. Schwack, M. Stammler, G. Poll, A. Reuter, Comparison of Life Calculations for Oscillating Bearings Considering Individual Pitch Control in Wind Turbines, in: J. Phys. Conf. Ser., 2016. doi:10.1088/1742-6596/753/11/112013.

3. M. Stammler, F. Schwack, N. Bader, A. Reuter, G. Poll, Friction torque of wind-turbine pitch bearings – comparison of experimental results with available models, Wind Energ. Sci. 3 (2018) 97–105. doi:10.5194/wes-3-97-2018

4. F. Schwack, F. Prigge, G. Poll, Finite element simulation and experimental analysis

of false brinelling and fretting corrosion, Tribol. Int. 126 (2018) 352–362. doi: 10.1016/j.triboint.2018.05.013.

5. SKF, Official website, http://www.skf.com/us/products/bearings-units-housings/super-precision-bearings/principles/design-considerations/system-rigidity/bearing-stiffness/index.html (2018/05).

6. S. Zupan, I. Prebil, Carrying angle and carrying capacity of a large single row ball bearing as a function of geometry parameters of the rolling contact and the supporting structure stiffness, Mech. Mach. Theory. 36 (2001) 1087–1103. doi:10.1016/S0094-114X(01)00044-1.

7. J.I. Amasorrain, X. Sagartzazu, J. Damián, Load distribution in a four contact-point slewing bearing, Mech. Mach. Theory. 38 (2003) 479–496. doi:10.1016/S0094-114X(03)00003-X.

8. T.A. Harris, M.N. Kotzalas, Rolling Bearing Analysis: Essential Concepts of Bearing Technology, 2006.

9. L. Houpert, A Uniform Analytical Approach for Ball and Roller Bearings Calculations, J. Tribol. (1997).

10. T. Lim, R. Singh, Vibration transmission through rolling element bearings, part I: Bearing stiffness formulation, J. Sound Vib. 139 (1990) 179–199.

11. X. Hernot, M. Sartor, J. Guillot, Calculation of the Stiffness Matrix of Angular Contact Ball Bearings by Using the Analytical Approach, J. Mech. Des. 122 (2000).

12. H.-V. Liew, T. Lim, Analysis of time-varying rolling element bearing characteristics, J. Sound Vib. 283 (2005) 1163–1179.

13. D. Noel, S. Le Loch, M. Ritou, B. Furet, Complete Analytical Expression of the Stiffness Matrix of Angular Contact Ball Bearings, J. Tribol. 135 (2013) 1–8.

14. M. Olave, X. Sagartzazu, J. Damian, A. Serna, Design of Four Contact-Point Slewing Bearing With a New Load Distribution Procedure to Account for Structural Stiffness, J. Mech. Des. 132 (2010) 21006. doi:10.1115/1.4000834.

15. Y. Guo, R. Parker, Stiffness matrix calculation of rolling element bearings using a finite element/contact mechanics model, Mech. Mach. Theory. 51 (2012) 32–45.

16. T. Smolnicki, E. Rusiński, Superelement-Based Modeling of Load Distribution in Large-Size Slewing Bearings, J. Mech. Des. 129 (2007) 459. doi:10.1115/1.2437784.

17. A. Daidié, Z. Chaib, A. Ghosn, 3D Simplified Finite Elements Analysis of Load and Contact Angle in a Slewing Ball Bearing, J. Mech. Des. 130 (2008) 82601. doi:10.1115/1.2918915.

18. ISO 76:2006. Rolling bearings - Static load ratings, 2006.

19. ISO/TR 10657:1991. Explanatory notes on ISO 76, 1991.

20. T.A. Harris, J.H. Rumbarger, C.P. Butterfield, Wind Turbine Design Guideline DG03: Yaw and Pitch Rolling Bearing Life. NREL/TP-500-42362, 2009.

21. Iraundi S.A., Slewing bearings catalogue, (2016).

22. SKF, Slewing bearings catalogue, (2015).

23. Rothe Erde, Product catalogue, (2016).

24. Schaeffler, Catalogue 404, (2012).

25. LYC, Products catalogue, (2010).

26. Rollix, Official website, http://www.rollix.com.

27. A. Joshi, B. Kachhia, H. Kikkari, M. Sridhar, D. Nelias, Running Torque of Slow Speed Two-Point and Four-Point Contact Bearings, Lubricants. 3 (2015) 181–196. doi:10.3390/lubricants3020181.

28. D. Gonçalves, S. Pinho, B. Graça, A. V. Campos, J.H.O. Seabra, Friction torque in thrust ball bearings lubricated with polymer greases of different thickener content, Tribol. Int. 96 (2016) 87–96. doi:10.1016/j.triboint.2015.12.017.

29. I. Heras, J. Aguirrebeitia, M. Abasolo, I. Coria, Additional material for the Wind Energy manuscript "An engineering approach for the estimation of slewing bearing stiffness in Wind Turbine Generators", Zenodo (2018). doi:10.5281/zenodo.1410453.